Two-Neutron Halo is Unveiled in ^{29}F

S. Bagchi,[1,2,3] R. Kanungo,[1,4,*] Y. K. Tanaka,[1,2,3] H. Geissel,[2,3] P. Doornenbal,[5] W. Horiuchi,[6] G. Hagen,[7,8] T. Suzuki,[9] N. Tsunoda,[10] D. S. Ahn,[5] H. Baba,[5] K. Behr,[2] F. Browne,[5] S. Chen,[5] M. L. Cortés,[5] A. Estradé,[11] N. Fukuda,[5] M. Holl,[1,4] K. Itahashi,[5] N. Iwasa,[12] G. R. Jansen,[7,13] W. G. Jiang,[8,7] S. Kaur,[1,14] A. O. Macchiavelli,[15] S. Y. Matsumoto,[16] S. Momiyama,[17] I. Murray,[5,18] T. Nakamura,[19] S. J. Novario,[8,7] H. J. Ong,[20,†] T. Otsuka,[5,17] T. Papenbrock,[8,7] S. Paschalis,[21] A. Prochazka,[2] C. Scheidenberger,[2,3] P. Schrock,[22] Y. Shimizu,[5] D. Steppenbeck,[5,22] H. Sakurai,[5,17] D. Suzuki,[5] H. Suzuki,[5] M. Takechi,[23] H. Takeda,[5] S. Takeuchi,[19] R. Taniuchi,[17,21] K. Wimmer,[17] and K. Yoshida[5]

[1]*Astronomy and Physics Department, Saint Mary's University, Halifax, Nova Scotia B3H 3C3, Canada*
[2]*GSI Helmholtzzentrum für Schwerionenforschung GmbH, D-64291 Darmstadt, Germany*
[3]*Justus-Liebig University, 35392 Giessen, Germany*
[4]*TRIUMF, Vancouver, British Columbia V6T 2A3, Canada*
[5]*RIKEN Nishina Center, Wako, Saitama 351-0198, Japan*
[6]*Department of Physics, Hokkaido University, Sapporo 060-0810, Japan*
[7]*Physics Division, Oak Ridge National Laboratory, Oak Ridge, Tennessee 37831, USA*
[8]*Department of Physics and Astronomy, University of Tennessee, Knoxville, Tennessee 37996, USA*
[9]*Department of Physics, Nihon University, Setagaya-ku, Tokyo 156-8550, Japan*
[10]*Center for Nuclear Study, University of Tokyo, Bunkyo-ku, Tokyo 113-0033, Japan*
[11]*Department of Physics, Central Michigan University, Mount Pleasant, Michigan 48859, USA*
[12]*Department of Physics, Tohoku University, Miyagi 980-8577, Japan*
[13]*National Center for Computational Sciences, Oak Ridge National Laboratory, Oak Ridge, Tennessee 37831, USA*
[14]*Department of Physics and Atmospheric Science, Dalhousie University, Halifax, Nova Scotia B3H 4R2, Canada*
[15]*Nuclear Science Division, Lawrence Berkeley National Laboratory, Berkeley, California 94720, USA*
[16]*Department of Physics, Kyoto University, Kyoto 606-8502, Japan*
[17]*Department of Physics, University of Tokyo, Bunkyo-ku, Tokyo 113-0033, Japan*
[18]*Institut de Physique Nucleaire, IN2P3, CNRS, Université Paris-Sud, Université Paris-Saclay, 91406 Orsay Cedex, France*
[19]*Department of Physics, Tokyo Institute of Technology, 2-12-1 O-Okayama, Meguro, Tokyo 152-8551, Japan*
[20]*RCNP, Osaka University, Mihogaoka, Ibaraki, Osaka 567 0047, Japan*
[21]*Department of Physics, University of York, Heslington, York YO10 5DD, United Kingdom*
[22]*Center for Nuclear Study, University of Tokyo, RIKEN Campus, Wako, Saitama 351-0198, Japan*
[23]*Graduate School of Science and Technology, Niigata University, Niigata 950-2102, Japan*

(Received 14 February 2020; revised manuscript received 17 April 2020; accepted 8 May 2020; published 5 June 2020)

We report the measurement of reaction cross sections ($\sigma_R^{\rm ex}$) of ^{27,29}F with a carbon target at RIKEN. The unexpectedly large $\sigma_R^{\rm ex}$ and derived matter radius identify ^{29}F as the heaviest two-neutron Borromean halo to date. The halo is attributed to neutrons occupying the $2p_{3/2}$ orbital, thereby vanishing the shell closure associated with the neutron number $N = 20$. The results are explained by state-of-the-art shell model calculations. Coupled-cluster computations based on effective field theories of the strong nuclear force describe the matter radius of ^{27}F but are challenged for ^{29}F.

DOI: 10.1103/PhysRevLett.124.222504

In atomic nuclei the strong force binds protons and neutrons into complex systems. Long-lived isotopes and β-stable nuclei exhibit a well-known shell structure [1,2]. However, in some nuclei with a large neutron excess an unusual type of structure emerges. In neutron-halo nuclei a large nuclear surface is formed that is almost entirely composed of neutrons [3,4]. Particularly interesting are so-called Borromean two-neutron halos [5]. These intriguing quantum systems consist of a bound state between a core nucleus and two neutrons, where any of the two-body subsystems are unbound. Examples known so far are ^{6}He, ^{11}Li, ^{14}Be, ^{17}B, and ^{22}C. A neutron-halo nucleus exhibits an enhanced root-mean-square matter radius ($R_m^{\rm ex}$) that can be extracted from the (unusually large) reaction cross section $\sigma_R^{\rm ex}$, which deviates from the known trend $R_m^{\rm ex} \propto A^{1/3}$ with mass number A. Some general conditions for halos are summarized in Ref. [6]. These exotic nuclei are intricately related to changes in the nuclear shell structure. In ^{11}Li, for example, the $N = 8$ shell gap vanishes with the intruder $2s_{1/2}$ orbital (35%–55%) that forms a Borromean halo in the last bound isotone [7,8].

Do all traditional neutron shell closures vanish into Borromean two-neutron halos? We address this question here for $N = 20$ by reporting the discovery of the heaviest

Borromean halo to date, and the first of its kind in the proton *sd* shell. The measured total reaction cross section σ_R^{ex} of the $N = 20$ nucleus ^{29}F is much larger than that of ^{27}F. This observation implies a two-neutron halo structure in ^{29}F, and the corresponding melting of the traditional $N = 20$ shell gap is due to the intrusion of the $2p_{3/2}$ orbital from a higher shell. Therefore, the two weakly bound neutrons experience only a small centrifugal barrier and have extended wave function to form the halo.

The weakening of the $N = 20$ shell gap was first hinted at from systematics of the two-neutron separation energies (S_{2n}) of sodium isotopes [9] and subsequently observed through the low excitation energy [10] and enhancement of reduced electric quadrupole transition probability [11] of ^{32}Mg. Since then a large number of investigations in neon to aluminum isotopes found intruder *pf*-shell components in level schemes [12,13], orbital configurations [14–17], and magnetic moment [18].

Monte Carlo shell model calculations [19] align well with these findings. It suggests that the monopole tensor interaction contributes to the shell quenching [20,21]. The high atomic number (Z) boundary of the quenched shell is drawn at the aluminum isotopes. The low-Z shore of this quenched shell remains undetermined. The observed lowest resonance state of ^{28}F can be explained by the USDB shell model interaction without appreciable need for any intruder orbitals from the *pf* shell [22] thereby concluding ^{28}F to follow normal shell ordering. Large-scale shell model calculations, however, predict the Borromean nucleus ^{29}F to be at the boundary of normal to quenched shells [23].

The boundary of bound nuclear landscape, the drip lines, are defined by the last bound isotopes or isotones [24]. We have few data on nuclei close to the neutron-drip line of the $N = 20$ isotones. In ^{29}F, the two-neutron separation energy $S_{2n} = 1.4(6)$ MeV is only known with a low precision [25]. The excited states of ^{27,29}F are observed [26] at 915 (12) keV and 1080(18) keV, respectively. The state in ^{29}F is slightly higher than shell-model prediction using the SDPF-M interaction [19] that includes the *pf* shell. A particle-rotor picture [27] also explains the ^{29}F spectrum, using a deformed ^{28}O core coupled to a proton in the $1d_{5/2}$ Nilsson multiplet. Regarding neutron halos, our knowledge is similarly limited. Carbon is the last known element to exhibit a Borromean two-neutron halo, and we do not know about any neutron halos in fluorine.

In this work, we report on the first measurement of the interaction cross sections (σ_I^{ex}) and determination of point matter radius of ^{27,29}F. The experiment was performed at the Radioactive Isotope Beam Factory operated by the RIKEN Nishina Center and the Center for Nuclear Study (CNS), University of Tokyo, Japan using the BigRIPS fragment separator and ZeroDegree spectrometer (ZDS) [28]. The experimental setup is shown in Fig. 1(a). The ^{27,29}F isotopes were produced from fragmentation of a ^{48}Ca beam with an average intensity of 570 pnA and an energy of 345A MeV interacting with a 10 mm thick rotating Be target. The isotopes of interest were separated from the various contaminant fragments using the BigRIPS fragment separator and identified [Fig. 1(b)] using the technique of in-flight energy deposit (ΔE), time of flight (TOF), and magnetic rigidity ($B\rho$). Achromatic wedge-shaped aluminium degraders of thicknesses 15 mm and 5 mm were used at the dispersive foci F1 and F5 [black inverted triangle in Fig. 1(a)], respectively, to spatially separate the beam contaminants. The $B\rho$ was determined from a position measurement with parallel plate avalanche counters (PPACs) [29] placed at the F3, F5, and F7 focal planes [green boxes in Fig. 1(a)]. An ionization chamber placed at F7 [pink box in Fig. 1(a)] provided the ΔE information. Plastic scintillator detectors of 3 mm thickness located at the F3 and F7 focal planes [white boxes in Fig. 1(a)] provided the TOF information. A 2.01 ± 0.01 g/cm^2-thick carbon reaction target was placed at F8 and was surrounded by the DALI2 NaI(Tl) array [30] for detecting gamma rays from the reactions. The average beam rates onto the F8 target were 314 pps and 78 pps, whereas the beam energies before the F8 target were 250A MeV and 255A MeV for ^{27}F and ^{29}F, respectively. In the event selection of fluorine isotopes, the relative contribution from Ne isotopes was $\leq 2 \times 10^{-9}$.

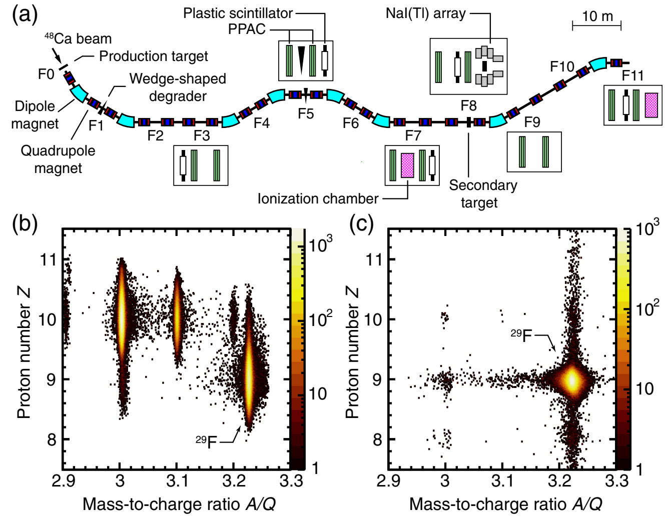

FIG. 1. (a) Schematic view of the experimental setup. The nuclei ^{27,29}F are transported from the focal plane F0 to F8, where the reaction target is located. Unreacted ^{29}F is identified using the ZDS from F8 to F11. Particle identification (b) before the carbon reaction target at F8 and (c) after the target at F11 with ^{29}F events selected before the target.

The σ_I^{ex} of the ^{A}F nuclei were measured via the transmission technique where the number of the incident nuclei (N_{in}) is obtained from an event-by-event counting at F7 and F8. After interaction with a carbon reaction target at F8, the unreacted ^{A}F (N_{out}) were counted at the F11 focal plane.

The σ_I was then obtained from the relation $\sigma_I^{ex} = t^{-1}\ln(T_{t\text{-out}}/T_{t\text{-in}})$, where $T_{t\text{-in}}$ and $T_{t\text{-out}}$ are the ratios of N_{out}/N_{in} with and without the reaction target, respectively, and t is the areal thickness of the target. Empty-target measurements were needed in order to take into account the losses due to interactions with residual materials in the beam-line and detection efficiencies. Constant transmission throughout the ZDS was obtained by restricting the phase space in x, y, and momentum directions before the reaction target at F8.

The unreacted ^{27,29}F residues were analyzed using the ZDS. The ΔE of these ions was measured using a Multi-Sampling Ionization Chamber (MUSIC) [31] detector [pink box in Fig. 1(a)] placed at the final achromatic focal plane F11 of the ZDS. The TOF was measured between two plastic scintillators having thicknesses 3 mm and 1 mm placed at the achromatic focal planes F8 and F11, respectively. The $B\rho$ was determined from the PPACs placed at the dispersive focal plane F9 and final focus F11. Figure 1(c) shows the particle identification obtained in the ZDS for events selected as ^{29}F before the reaction target at F8. The resolution of Z is obtained to be 0.2 (FWHM) and that of A/q for the F isotopes is 0.013 (FWHM).

The reaction cross section σ_R^{ex} is the sum of σ_I^{ex} and the inelastic scattering cross section ($\sigma_{inel,bs}$) to bound excited states. No gamma rays from inelastic scattering were observed. The efficiency of 1 MeV γ-ray detection was ~20%. The inelastic scattering γ-ray spectrum in Ref. [32] for ^{20}C yields a cross section of ~3 mb. Therefore, non-observation of a γ-ray peak places an upper limit of $\sigma_{inel,bs}$ to less than 1 mb for ^{27,29}F. Hence, $\sigma_R^{ex} \approx \sigma_I^{ex}$. The σ_R^{ex} for ^{27,29}F, 1243(14) mb and 1396(28) mb, respectively (red filled circles), and those for $^{19-26}$F from Ref. [33] (open blue squares), presented in Fig. 2, show a steep increase of about 12(2)% for ^{29}F revealing the presence of a two-neutron halo. This increase in σ_R^{ex} is similar to that found for ^{22}C [32].

The σ_R are calculated from the Glauber model with the nucleon-target profile function and a harmonic oscillator density for the ^{12}C target (see Supplemental Material for further details [34]). For ^{27,29}F we consider harmonic oscillator densities with several oscillator width parameters that yield different point-matter radii for these nuclei. Using each of these densities we evaluate the σ_R with the Glauber model. The calculated σ_R are compared to the measured σ_R^{ex} to extract the experimental R_m^{ex} of 3.15 ± 0.04 fm and 3.50 ± 0.07 fm for ^{27}F and ^{29}F, respectively. The results obtained are also consistent with a two-parameter Fermi density function. The large increase of R_m^{ex} by about 11(3)% for ^{29}F compared to ^{27}F is consistent with a two-neutron halo formation in the $N = 20$ isotone at the drip line and is well above the 2.4% increase expected from the $A^{1/3}$ rule. A large root-mean-square halo radius of 6.6 fm for ^{29}F is derived considering the proton radii in ^{27}F and ^{29}F to be similar. The difference between the R_m^{ex} of ^{29}F and its core ^{27}F is 0.35 ± 0.08 fm which is similar to the two-neutron halo nuclei ^{14}Be, ^{17}B [48], and ^{22}C [32].

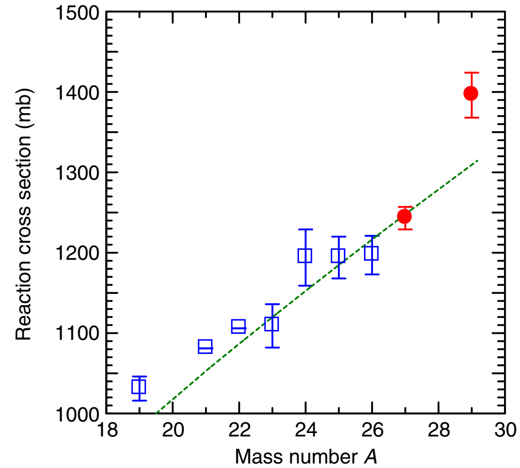

FIG. 2. Measured reaction cross sections of fluorine isotopes with a carbon target at $E/A \approx 240$ MeV. The red filled circles are data of the present work. The open blue squares are from Ref. [33]. The data show statistical and systematic uncertainties. The dashed line shows the trend of $A^{2/3}$ relative evolution normalized for best fit to $^{19-27}$F.

To assess the neutron orbitals associated with the halo, we perform Glauber calculation with a density of ^{29}F as $^{27}\text{F} + n + n$. The large increase of the matter radii from ^{27}F to ^{29}F indicates a strong component of the intruder $2p_{3/2}$ orbital. Its centrifugal barrier being a factor of 3 lower than the $1d_{3/2}$ orbital facilitates an extended wave function. The large extension becomes possible due to the small S_{2n} in ^{29}F [25] approaching the effective threshold as shown for the higher angular momentum orbital in Ref. [49]. To obtain the ^{29}F density, we assume mixing of the $(1d_{3/2})^2$ and $(2p_{3/2})^2$ configurations with their wave functions generated from the Woods-Saxon potential using a single-neutron energy of $S_{2n}/2 = 0.7(3)$ MeV [25] (see Supplemental Material [34] for more details). Figure 3 shows the result of the mixing according to $\sigma_R = \alpha \times \sigma_R(2p_{3/2}) + (1-\alpha) \times \sigma_R(1d_{3/2})$ with α being the occupation probability normalized to unity. For ^{29}F, the consistency between σ_R^{ex} and the σ_R calculated with the Glauber model requires $\alpha = 0.54$–1.0 for $S_{2n}/2 = 0.7$ MeV, indicating that the halo is driven by the lowering of the $2p_{3/2}$ orbital and the $N = 20$ and 28 shell closures vanishing. The uncertainty in S_{2n} gives a lower limit of $\alpha = 0.36$ (Fig. 3). One can also describe ^{27}F as a $^{26}\text{F} + n$ configuration (where the ^{26}F core radius R_m is taken to reproduce its σ_R^{ex}). In this approach, the neutron occupation in the $1d_{3/2}$ orbital alone is able to explain σ_R^{ex} of ^{27}F, suggesting a very small contribution of the intruder pf orbitals.

In order to gain further insight into the shell structure driving the halo formation, the matter radii are evaluated by

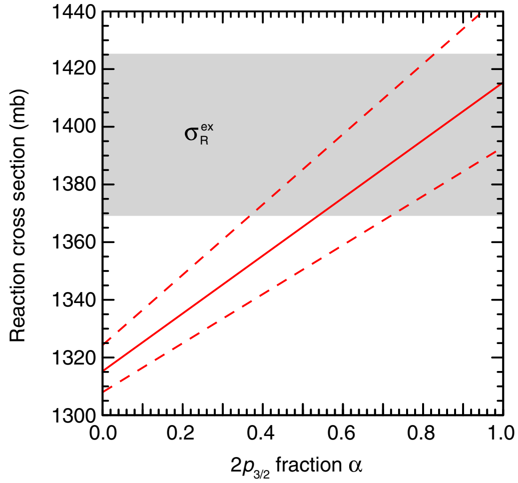

FIG. 3. The red lines show Glauber calculation of σ_R of ^{29}F + C with ^{27}F + n + n densities at $E/A = 246$ MeV (midtarget energy) for different fractions (α), (see text for definition) of neutrons in the $2p_{3/2}$ orbital. The solid (dashed) lines are for $S_{2n}/2$= 0.7(3) MeV. The horizontal shaded band corresponds to the measured $\sigma_R^{\rm ex}$.

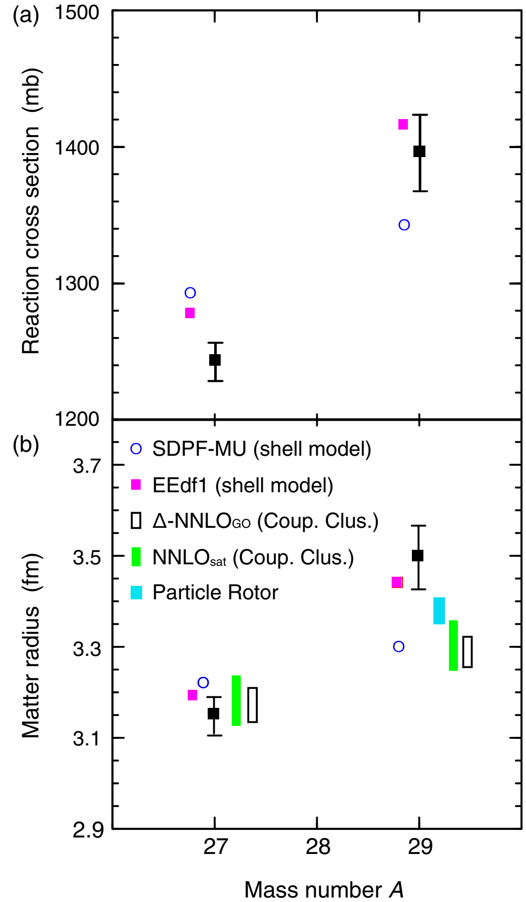

FIG. 4. Comparison between the experimental values for $\sigma_R^{\rm ex}$ and $R_m^{\rm ex}$ and various theoretical results. The data include statistical and systematic uncertainties. (a) Comparison of measured $\sigma_R^{\rm ex}$ (black filled squares) with Glauber calculations using density distributions from the shell model based on the SDPF-MU (open blue circles) and the EEdf1 (magenta square) interaction. (b) Comparison of derived $R_m^{\rm ex}$ for ^{27,29}F (black filled squares) with predictions from shell-model calculations using the SDPF-MU interaction (open blue circles) and the EEdf1 interaction (magenta squares). Coupled-cluster results based on the chiral NNLO$_{\rm sat}$ (Δ-NNLO$_{\rm GO}$) interaction are shown as a green band (open black-white band). The cyan band is the result from a particle-rotor model.

using occupation numbers obtained from shell-model calculations in the sd-pf shell. One calculation is performed with the SDPF-MU Hamiltonian [50]. For ^{27,29}F, radial wave functions are calculated in a Woods-Saxon potential (see Supplemental Material [34] for further details). The σ_R using these densities for ^{27,29}F are shown by open blue circles in Fig. 4(a). The resultant matter radii are 3.22 fm and 3.30 fm [open blue circles in Fig. 4(b)] for ^{27}F and ^{29}F, respectively. The corresponding neutron occupation numbers of the $1d_{3/2}$, $1f_{7/2}$, and $2p_{3/2}$ orbitals are predicted as 2.68, 0.90, and 0.56 in ^{29}F and 1.67, 0.48, and 0.24 in ^{27}F. The underprediction of R_m and σ_R for ^{29}F can be traced back to unbound pf orbitals. These appear with a small component in the ground-state configuration while the $1d_{3/2}$ orbital is bound and has a larger component. The predicted first excited states in ^{27,29}F are at 1.48 MeV and 1.51 MeV, respectively, slightly higher than the data in Ref. [26].

Matter radii and σ_R are also evaluated with a microscopic interaction called EEdf1 [51] which has been derived [52] by the extended Kuo-Krenciglowa (EKK) method [53–56] from a chiral N^{3}LO interaction [57] and Fujita-Miyazawa three-body force [58] (magenta squares in Fig. 4). The sd and pf shells are more strongly mixed than by the SDPF-MU interaction, with neutron occupation numbers of the $1d_{3/2}$, $1f_{7/2}$, and $2p_{3/2}$ orbitals in ^{29}F (^{27}F) being 0.84, 2.19, and 1.26 (0.80, 1.08, and 0.67), respectively. The substantial contribution of the bound $2p_{3/2}$ orbital leads to the observed halo formation. The computed matter radius of 3.44 fm for ^{29}F agrees with the data, while that of ^{27}F is 3.19 fm [magneta squares in Fig. 4(b)]. We note that the $1d_{3/2}$ orbital is unbound with the EEdf1 interaction. It predicts the first and second excited states in ^{27}F at 0.14 MeV and 1.42 MeV, respectively. Those in ^{29}F are predicted at 0.09 MeV and 1.08 MeV, respectively, the latter being in agreement with the observed γ-ray transition [26]. This suggests the first excited state could be below the detection threshold. The low excitation energies in ^{29}F align with the quenching of the $N = 20$ shell closure.

We also performed *ab initio* coupled-cluster calculations [59–65] for the binding energies and matter radii of ^{27,29}F. These computations are based on a deformed reference state. We used two different interactions from chiral effective field theory [66–68] that consist of nucleon-nucleon and three-nucleon forces, namely NNLO$_{\rm sat}$ [69]

and Δ-NNLO$_{GO}$(450) [70]. Both interactions are constrained by nuclear saturation properties (see Supplemental Material [34] for further details). The coupled-cluster results for the matter radius of ^{27}F agree with the data, while those for ^{29}F are smaller than the data. Error ranges reflect uncertainties with respect to model-space sizes and extrapolation of radii. In our deformed reference state, the neutrons closest to the Fermi surface occupy positive parity states, dominantly associated with the $1d_{3/2}$ orbital. These states were self-consistently selected by the Hartree-Fock method. A halo in ^{29}F would require neutrons to occupy the $2p_{3/2}$ orbital. Thus, the coupled-cluster computations lead to smaller radii pointing to shortcomings in the employed interactions.

The matter radius is also estimated for ^{29}F using the particle-rotor model [27], assuming a prolate ellipsoidal shape. This approach hints to a possible effective deformed ^{28}O core (with deformation $\varepsilon_2 \approx 0.16^{+0.15}_{-0.2}$) [27], supportive of a breakdown of the $N = 20$ shell. The resulting radius is slightly lower than the data (cyan bar in Fig. 4).

While this Letter was under review, the matter radii of $^{27-31}$F were predicted in a Gamow Shell Model framework [71]. The prediction for ^{27}F is slightly higher and that of ^{29}F is slightly lower than the data presented here. Future experiments will aim to assess the halo predicted for ^{31}F in Ref. [71] and a pairing antihalo effect predicted in Ref. [72].

The present work shows that a small neutron separation energy (∼1 MeV), and tensor force effects lead to a p-wave halo in ^{29}F, one proton above conventional doubly closed shell $Z = 8$ and $N = 20$. This is analogous to an s-wave halo in ^{11}Li, one proton above $Z = 2$ and $N = 8$. Both ^{29}F and ^{11}Li are at the neutron drip line with the respective conventional doubly magic cores, ^{28}O and ^{10}He, being unbound. The extended wave functions of such weakly bound s or p orbitals in the ground states of nuclei around the $N = 50$, 82, and 126 shells will lead to greater probability of neutron capture [73] thereby impacting the flow of the rapid neutron capture process. One-neutron halos and quenching of the $N = 50$ shell gap are predicted in Cr and Fe isotopes [74] and two-neutron halo in Ca isotopes [75]. A recent study of ^{207}Hg beyond $N = 126$ shows the normal shell ordering to persist [76]. Calculations with a Woods-Saxon potential however predict a shell gap quenching due to weak binding in more neutron-rich $N = 126$ isotones. This follows the trend in light nuclei discussed in Refs. [77,78].

In conclusion, we identified a new two-neutron Borromean halo—the first of this kind in the proton sd shell—in the $N = 20$ drip-line nucleus ^{29}F. This observation was from the large difference in the reaction cross sections σ_R^{ex} measured for ^{27,29}F. Assuming similar proton distributions in ^{27}F and ^{29}F yields a large root-mean-square halo radius of 6.6 fm for ^{29}F. The emergence of the halo leads to vanishing of the $N = 20$ shell closure with contribution of the $2p_{3/2}$ orbital. This weakens the $N = 28$ shell gap as well. The disappearance of the conventional shell gap and emergence of the halo challenges *ab initio* computations and will trigger further experiments characterizing this halo.

The authors gratefully thank the RIKEN Rare Isotope Beam Factory for delivering the ^{48}Ca beam with unprecedented high intensity. The support from NSERC Canada is gratefully acknowledged. This work was also supported by JSPS KAKENHI Grants No. 16H02179, No. 18H05404, UK STFC under Contract No. ST/P003885/1, the U.S. Department of Energy, Office of Science, Office of Nuclear Physics under Contract No. DE-AC02-05CH11231 (LBNL). The work was supported in part by the Office of Nuclear Physics, U.S. Department of Energy, under Grants No. DE-SC0018223 (SciDAC-4 NUCLEI Collaboration), No. DE-FG02-96ER40963, and by the Field Work Proposal ERKBP72 at Oak Ridge National Laboratory (ORNL). Computer time was provided by the Innovative and Novel Computational Impact onTheory and Experiment (INCITE) program. This research used resources of the Oak Ridge Leadership Computing Facility and of the Compute and Data Environment for Science (CADES) located at ORNL, which is supported by the Office of Science of the Department of Energy under Contract No. DE-AC05-00OR22725. R. K. acknowledges the JSPS invitational fellowship program for short term research stay in Japan at the Tokyo Institute of Technology.

*ritu@triumf.ca
†Present Address: Institute of Modern Physics, Chinese Academy of Sciences, Lanzhou 730000, China.

[1] M. G. Mayer, Nuclear configurations in the spin-orbit coupling model. i. empirical evidence, Phys. Rev. **78**, 16 (1950).
[2] O. Haxel, J. H. D. Jensen, and H. E. Suess, On the "magic numbers" in nuclear structure, Phys. Rev. **75**, 1766 (1949).
[3] I. Tanihata, H. Hamagaki, O. Hashimoto, Y. Shida, N. Yoshikawa, K. Sugimoto, O. Yamakawa, T. Kobayashi, and N. Takahashi, Measurements of Interaction Cross Sections and Nuclear Radii in the Light p-Shell Region, Phys. Rev. Lett. **55**, 2676 (1985).
[4] P. G. Hansen and B. Jonson, The neutron halo of extremely neutron-rich nuclei, Europhys. Lett. **4**, 409 (1987).
[5] J. S. Vaagen, D. K. Gridnev, H. Heiberg-Andersen, B. V. Danilin, S. N. Ershov, V. I. Zagrebaev, I. J. Thompson, M. V. Zhukov, and J. M. Bang, Borromean halo nuclei, Phys. Scr. **T88**, 209 (2000).
[6] A. S. Jensen and K. Riisager, Towards necessary and sufficient conditions for halo occurrence, Phys. Lett. B **480**, 39 (2000).
[7] H. Simon *et al.*, Direct Experimental Evidence for Strong Admixture of Different Parity States in ^{11}Li, Phys. Rev. Lett. **83**, 496 (1999).

[8] I. Tanihata *et al.*, Measurement of the Two-Halo Neutron Transfer Reaction $^1H(^{11}Li, ^9Li)^3H$ at 3*A* MeV, Phys. Rev. Lett. **100**, 192502 (2008).

[9] C. Thibault, R. Klapisch, C. Rigaud, A. M. Poskanzer, R. Prieels, L. Lessard, and W. Reisdorf, Direct measurement of the masses of ^{11}Li and $^{26–32}$Na with an on-line mass spectrometer, Phys. Rev. C **12**, 644 (1975).

[10] C. Détraz, D. Guillemaud, G. Huber, R. Klapisch, M. Langevin, F. Naulin, C. Thibault, L. C. Carraz, and F. Touchard, Beta decay of $^{26–32}$Na and their descendants, Phys. Rev. C **19**, 164 (1979).

[11] T. Motobayashi, Y. Ikeda, K. Ieki, M. Inoue, N. Iwasa, T. Kikuchi, M. Kurokawa, S. Moriya, S. Ogawa, H. Murakami, S. Shimoura, Y. Yanagisawa, T. Nakamura, Y. Watanabe, M. Ishihara, T. Teranishi, H. Okuno, and R. F. Casten, Large deformation of the very neutron-rich nucleus ^{32}Mg from intermediate-energy Coulomb excitation, Phys. Lett. B **346**, 9 (1995).

[12] V. Tripathi, S. L. Tabor, P. F. Mantica, C. R. Hoffman, M. Wiedeking, A. D. Davies, S. N. Liddick, W. F. Mueller, T. Otsuka, A. Stolz, B. E. Tomlin, Y. Utsuno, and A. Volya, ^{29}Na: Defining the Edge of the Island of Inversion for $Z = 11$, Phys. Rev. Lett. **94**, 162501 (2005).

[13] P. Doornenbal *et al.*, Spectroscopy of ^{32}Ne and the "Island of Inversion", Phys. Rev. Lett. **103**, 032501 (2009).

[14] M. Takechi *et al.*, Interaction cross sections for Ne isotopes towards the island of inversion and halo structures of ^{29}Ne and ^{31}Ne, Phys. Lett. B **707**, 357 (2012).

[15] T. Nakamura *et al.*, Deformation-Driven *p*-Wave Halos at the Drip Line: ^{31}Ne, Phys. Rev. Lett. **112**, 142501 (2014).

[16] N. Kobayashi *et al.*, One-neutron removal from ^{29}Ne: Defining the lower limits of the island of inversion, Phys. Rev. C **93**, 014613 (2016).

[17] H. N. Liu *et al.*, Intruder configurations in the ground state of ^{30}Ne, Phys. Lett. B **767**, 58 (2017).

[18] G. Neyens, M. Kowalska, D. Yordanov, K. Blaum, P. Himpe, P. Lievens, S. Mallion, R. Neugart, N. Vermeulen, Y. Utsuno, and T. Otsuka, Measurement of the Spin and Magnetic Moment of ^{31}Mg: Evidence for a Strongly Deformed Intruder Ground State, Phys. Rev. Lett. **94**, 022501 (2005).

[19] Y. Utsuno, T. Otsuka, T. Mizusaki, and M. Honma, Varying shell gap and deformation in $N \sim 20$ unstable nuclei studied by the Monte Carlo shell model, Phys. Rev. C **60**, 054315 (1999).

[20] T. Otsuka, T. Suzuki, R. Fujimoto, H. Grawe, and Y. Akaishi, Evolution of Nuclear Shells Due to the Tensor Force, Phys. Rev. Lett. **95**, 232502 (2005).

[21] T. Otsuka, A. Gade, O. Sorlin, T. Suzuki, and Y. Utsuno, Evolution of shell structure in exotic nuclei, Rev. Mod. Phys. **92**, 015002 (2020).

[22] G. Christian *et al.*, Exploring the Low-*Z* Shore of the Island of Inversion at $N = 19$, Phys. Rev. Lett. **108**, 032501 (2012).

[23] E. Caurier, F. Nowacki, and A. Poves, Merging of the islands of inversion at $N = 20$ and $N = 28$, Phys. Rev. C **90**, 014302 (2014).

[24] P. G. Hansen and J. A. Tostevin, Direct reactions with exotic nuclei, Annu. Rev. Nucl. Part. Sci. **53**, 219 (2003).

[25] L. Gaudefroy, W. Mittig, N. A. Orr, S. Varet, M. Chartier, P. Roussel-Chomaz, J. P. Ebran, B. Fernández-Domínguez, G. Frémont, P. Gangnant, A. Gillibert, S. Grévy, J. F. Libin, V. A. Maslov, S. Paschalis, B. Pietras, Y.-E. Penionzhkevich, C. Spitaels, and A. C. C. Villari, Direct Mass Measurements of ^{19}B, ^{22}C, ^{29}F, ^{31}Ne, ^{34}Na and Other Light Exotic Nuclei, Phys. Rev. Lett. **109**, 202503 (2012).

[26] P. Doornenbal, H. Scheit, S. Takeuchi, Y. Utsuno, N. Aoi, K. Li, M. Matsushita, D. Steppenbeck, H. Wang, H. Baba, E. Ideguchi, N. Kobayashi, Y. Kondo, J. Lee, S. Michimasa, T. Motobayashi, T. Otsuka, H. Sakurai, M. Takechi, Y. Togano, and K. Yoneda, Low-*Z* shore of the "island of inversion" and the reduced neutron magicity toward ^{28}O, Phys. Rev. C **95**, 041301(R) (2017).

[27] A. O. Macchiavelli, H. L. Crawford, P. Fallon, C. M. Campbell, R. M. Clark, M. Cromaz, M. D. Jones, I. Y. Lee, and M. Salathe, Structure of ^{29}F in the rotation-aligned coupling scheme of the particle-rotor model, Phys. Lett. B **775**, 160 (2017).

[28] T. Kubo, D. Kameda, H. Suzuki, N. Fukuda, H. Takeda, Y. Yanagisawa, M. Ohtake, K. Kusaka, K. Yoshida, N. Inabe, T. Ohnishi, A. Yoshida, K. Tanaka, and Y. Mizoi, BigRIPS separator and ZeroDegree spectrometer at RIKEN RI Beam Factory, Prog. Theor. Exp. Phys. (**2012**), 03C003.

[29] H. Kumagai, T. Ohnishi, N. Fukuda, H. Takeda, D. Kameda, N. Inabe, K. Yoshida, and T. Kubo, Development of parallel plate avalanche counter (ppac) for BIGRIPS fragment separator, Nucl. Instrum. Methods Phys. Res., Sect. B **317**, 717 (2013).

[30] S. Takeuchi, T. Motobayashi, Y. Togano, M. Matsushita, N. Aoi, K. Demichi, H. Hasegawa, and H. Murakami, Dali2: A NaI(Tl) detector array for measurements of γ rays from fast nuclei, Nucl. Instrum. Methods Phys. Res., Sect. A **763**, 596 (2014).

[31] A. Stolz, T. Faestermann, J. Friese, P. Kienle, H.-J. Körner, M. Münch, R. Schneider, E. Wefers, K. Zeitelhack, K. Sümmerer, H. Geissel, J. Gerl, G. Münzenberg, C. Schlegel, R. S. Simon, H. Weick, M. Hellström, M. N. Mineva, and P. Thirolf, Projectile fragmentation of ^{112}Sn at $E_{\mathrm{lab}} = 1A$ GeV, Phys. Rev. C **65**, 064603 (2002).

[32] Y. Togano *et al.*, Interaction cross section study of the two-neutron halo nucleus ^{22}C, Phys. Lett. B **761**, 412 (2016).

[33] A. Homma *et al.*, Measurements of interaction cross sections for $^{19–27}$F isotopes, in *Proceedings of the 14th International Symposium on Nuclei in the Cosmos (NIC2016)* (JPS Conference Proceedings, Japan, 2017) p. 021010.

[34] See Supplemental Material at http://link.aps.org/supplemental/10.1103/PhysRevLett.124.222504 for details on theoretical models, which includes Refs. [35–47].

[35] B. Abu-Ibrahim and Y. Suzuki, Utility of nucleon-target profile function in cross section calculations, Phys. Rev. C **61**, 051601(R) (2000).

[36] W. Horiuchi, Y. Suzuki, B. Abu-Ibrahim, and A. Kohama, Systematic analysis of reaction cross sections of carbon isotopes, Phys. Rev. C **75**, 044607 (2007).

[37] B. Abu-Ibrahim, W. Horiuchi, A. Kohama, and Y. Suzuki, Reaction cross sections of carbon isotopes incident on a proton, Phys. Rev. C **77**, 034607 (2008).

[38] I. Angeli and K. P. Marinova, Table of experimental nuclear ground state charge radii: An update, At. Data Nucl. Data Tables **99**, 69 (2013).

[39] W. Horiuchi, Y. Suzuki, P. Capel, and D. Baye, Probing the weakly-bound neutron orbit of ^{31}Ne with total reaction and one-neutron removal cross sections, Phys. Rev. C **81**, 024606 (2010).

[40] M. Wang, G. Audi, F. G. Kondev, W. J. Huang, S. Naimi, and X. Xu, The AME2016 atomic mass evaluation (II). tables, graphs and references, Chin. Phys. C **41**, 030003 (2017).

[41] A. Ekström, G. Hagen, T. D. Morris, T. Papenbrock, and P. D. Schwartz, Δ isobars and nuclear saturation, Phys. Rev. C **97**, 024332 (2018).

[42] G. Hagen, A. Ekström, C. Forssén, G. R. Jansen, W. Nazarewicz, T. Papenbrock, K. A. Wendt, S. Bacca, N. Barnea, B. Carlsson, C. Drischler, K. Hebeler, M. Hjorth-Jensen, M. Miorelli, G. Orlandini, A. Schwenk, and J. Simonis, Neutron and weak-charge distributions of the ^{48}Ca nucleus, Nat. Phys. **12**, 186 (2016).

[43] R. Kanungo *et al.*, Proton Distribution Radii of $^{12–19}$C Illuminate Features of Neutron Halos, Phys. Rev. Lett. **117**, 102501 (2016).

[44] T. Duguet, V. Somà, S. Lecluse, C. Barbieri, and P. Navrátil, *Ab initio* calculation of the potential bubble nucleus ^{34}Si, Phys. Rev. C **95**, 034319 (2017).

[45] A. Tichai, J. Müller, K. Vobig, and R. Roth, Natural orbitals for ab initio no-core shell model calculations, Phys. Rev. C **99**, 034321 (2019).

[46] Y. S. Lee, S. A. Kucharski, and R. J. Bartlett, A coupled cluster approach with triple excitations, J. Chem. Phys. **81**, 5906 (1984).

[47] Ik J. Shin, Y. Kim, P. Maris, J. P. Vary, C. Forssén, J. Rotureau, and N. Michel, Ab initio no-core solutions for ^{6}Li, J. Phys. G **44**, 075103 (2017).

[48] A. Ozawa, T. Suzuki, and I. Tanihata, Nuclear size and related topics, Nucl. Phys. **A693**, 32 (2001).

[49] C. R. Hoffman, B. P. Kay, and J. P. Schiffer, Ordering of the $0d_{5/2}$ and $1s_{1/2}$ proton levels in light nuclei, Phys. Rev. C **94**, 024330 (2016).

[50] Y. Utsuno, T. Otsuka, B. A. Brown, M. Honma, T. Mizusaki, and N. Shimizu, Shape transitions in exotic Si and S isotopes and tensor-force-driven Jahn-Teller effect, Phys. Rev. C **86**, 051301(R) (2012).

[51] B. Fernández-Dom'nguez *et al.*, Re-examining the transition into the $N = 20$ island of inversion: Structure of ^{30}Mg, Phys. Lett. B **779**, 124 (2018).

[52] N. Tsunoda, T. Otsuka, N. Shimizu, M. Hjorth-Jensen, K. Takayanagi, and T. Suzuki, Exotic neutron-rich medium-mass nuclei with realistic nuclear forces, Phys. Rev. C **95**, 021304(R) (2017).

[53] E. M. Krenciglowa and T. T. S. Kuo, Convergence of effective hamiltonian expansion and partial summations of folded diagrams, Nucl. Phys. **A235**, 171 (1974).

[54] K. Takayanagi, Effective interaction in non-degenerate model space, Nucl. Phys. **A852**, 61 (2011).

[55] K. Takayanagi, Effective Hamiltonian in the extended Krenciglowa-Kuo method, Nucl. Phys. **A864**, 91 (2011).

[56] N. Tsunoda, K. Takayanagi, M. Hjorth-Jensen, and T. Otsuka, Multi-shell effective interactions, Phys. Rev. C **89**, 024313 (2014).

[57] D. R. Entem and R. Machleidt, Accurate charge-dependent nucleon-nucleon potential at fourth order of chiral perturbation theory, Phys. Rev. C **68**, 041001(R) (2003).

[58] J. Fujita and H. Miyazawa, Pion theory of three-body forces, Prog. Theor. Phys. **17**, 360 (1957).

[59] F. Coester and H. Kümmel, Short-range correlations in nuclear wave functions, Nucl. Phys. **17**, 477 (1960).

[60] H. Kümmel, K. H. Lührmann, and J. G. Zabolitzky, Many-fermion theory in expS- (or coupled cluster) form, Phys. Rep. **36**, 1 (1978).

[61] R. F. Bishop, An overview of coupled cluster theory and its applications in physics, Theor. Chim. Acta **80**, 95 (1991).

[62] B. Mihaila and J. H. Heisenberg, Microscopic Calculation of the Inclusive Electron Scattering Structure Function in ^{16}O, Phys. Rev. Lett. **84**, 1403 (2000).

[63] D. J. Dean and M. Hjorth-Jensen, Coupled-cluster approach to nuclear physics, Phys. Rev. C **69**, 054320 (2004).

[64] R. J. Bartlett and M. Musiał, Coupled-cluster theory in quantum chemistry, Rev. Mod. Phys. **79**, 291 (2007).

[65] G. Hagen, T. Papenbrock, M. Hjorth-Jensen, and D. J. Dean, Coupled-cluster computations of atomic nuclei, Rep. Prog. Phys. **77**, 096302 (2014).

[66] U. Van Kolck, Effective field theory of nuclear forces, Prog. Part. Nucl. Phys. **43**, 337 (1999).

[67] E. Epelbaum, H.-W. Hammer, and Ulf-G. Meißner, Modern theory of nuclear forces, Rev. Mod. Phys. **81**, 1773 (2009).

[68] R. Machleidt and D. R. Entem, Chiral effective field theory and nuclear forces, Phys. Rep. **503**, 1 (2011).

[69] A. Ekström, B. D. Carlsson, K. A. Wendt, C. Forssén, M. Hjorth Jensen, R. Machleidt, and S. M. Wild, Statistical uncertainties of a chiral interaction at next-to-next-to leading order, J. Phys. G **42**, 034003 (2015).

[70] C. G. Payne, S. Bacca, G. Hagen, W. G. Jiang, and T. Papenbrock, Coherent elastic neutrino-nucleus scattering on ^{40}Ar from first principles, Phys. Rev. C **100**, 061304(R) (2019).

[71] N. Michel, J. G. Li, F. R. Xu, and W. Zuo, Two-neutron halo structure of ^{31}F, Phys. Rev. C **101**, 031301(R) (2020).

[72] H. Masui, W. Horiuchi, and M. Kimura, Two-neutron halo structure of ^{31}F and a novel pairing antihalo effect, Phys. Rev. C **101**, 041303(R) (2020).

[73] G. J. Mathews, A. Mengoni, F.-K. Thielemann, and W. A. Fowler, Neutron capture rates in the *r* process: The role of direct radiative capture, Astrophys. J. **270**, 740 (1983).

[74] I. Hamamoto, Examining possible neutron-halo nuclei heavier than ^{37}Mg, Phys. Rev. C **95**, 044325 (2017).

[75] G. Hagen, P. Hagen, H.-W. Hammer, and L. Platter, Efimov Physics Around Neutron-rich ^{60}Ca Isotope, Phys. Rev. Lett. **111**, 132501 (2013).

[76] T. L. Tang *et al.*, First Exploration of Neutron Shell Structure Below Lead and Beyond $N = 126$, Phys. Rev. Lett. **124**, 062502 (2020).

[77] A. Ozawa, T. Kobayashi, T. Suzuki, K. Yoshida, and I. Tanihata, New Magic Number, $N = 16$, Near the Neutron Drip Line, Phys. Rev. Lett. **84**, 5493 (2000).

[78] C. R. Hoffman, B. P. Kay, and J. P. Schiffer, Neutron *s* states in loosely bound nuclei, Phys. Rev. C **89**, 061305(R) (2014).